Thermostructural evaluation of poly(butylene adipate-co-terephthalate) /molybdenum trioxide nanocomposites through time domain nuclear magnetic resonance and other conventional techniques

Avaliação termo-estrutural de nanocompósitos de poli(adipato-co-tereftalato de butileno) / trióxido de molibdénio através de ressonância magnética nuclear no domínio do tempo e outras técnicas convencionais

DOI:10.34117/bjdv8n5-257

Recebimento dos originais: 21/03/2022
Aceitação para publicação: 29/04/2022

Lizandra Viana Maurat da Rocha
Mestre em Ciência e Tecnologia de Polímeros
Instituição: doutoranda no Instituto de Macromoléculas Professora Eloisa Mano (IMA/UFRJ)
Endereço: IMA/UFRJ, Av. Horácio Macedo 2030, bloco J, Centro de Tecnologia, Ilha do Fundão, Rio de Janeiro, RJ, Brasil, CEP: 21941-598
E-mail: lizandramaurat@nano.ufrj.br

Paulo Sérgio Rangel Cruz da Silva
Doutor em Ciência e Tecnologia de Polímeros
Instituição: Pesquisador do IMA
Endereço: IMA/UFRJ, Av. Horácio Macedo 2030, bloco J, Centro de Tecnologia, Ilha do Fundão, Rio de Janeiro, RJ, Brasil, CEP: 21941-598
E-mail: rangel@ima.ufrj.br

Maria Inês Bruno Tavares
Doutora em Ciência e Tecnologia de Polímeros
Instituição: Professora Titular e Diretora do IMA
Endereço: IMA/UFRJ, Av. Horácio Macedo 2030, bloco J, Centro de Tecnologia, Ilha do Fundão, Rio de Janeiro, RJ, Brasil, CEP: 21941-598
E-mail: mibt@ima.ufrj.br

ABSTRACT
In present study, poly(butylene adipate-co-terephthalate) (PBAT) nanocomposites films were prepared by solvent casting technique, using chloroform ($CHCl_3$) and containing different percentages (0-0.5 wt %) of molybdenum trioxide (MoO_3) nanoparticles (NPs). The microstructure and molecular dynamics of the PBAT and PBAT/MoO_3 films were characterized by X-ray diffraction (XRD) and time-domain nuclear magnetic resonance (TD-NMR). Films' thermal degradation was studied by using thermogravimetric analysis (TGA). Fourier transform infrared spectroscopy (FTIR) confirmed: no residual solvent or contaminants and polymer matrix integrity after the casting process. The results' matchup indicated that filler–polymer interaction was suitable and, thus, MoO_3NPs are potential candidates to be used as filler in PBAT matrices, especially in concentrations around 0.3 %.

Keywords: PBAT, MoO_3, Nanocomposite films, TD-NMR, structural properties.

ABSTRACT
No presente estudo, as películas de nanocompósitos de poli(adipato-co-tereftalato de butileno) (PBAT) foram preparadas por técnica de fundição por solventes, utilizando clorofórmio (CHCl3) e contendo diferentes percentagens (0-0,5 wt %) de trióxido de molibdénio (MoO3) nanopartículas (NPs). A microestrutura e a dinâmica molecular dos filmes PBAT e PBAT/MoO3 caracterizaram-se pela difracção de raios X (XRD) e pela ressonância magnética nuclear de domínio temporal (TD-NMR). A degradação térmica dos filmes foi estudada utilizando a análise termogravimétrica (TGA). A espectroscopia de infravermelho por transformação de Fourier (FTIR) confirmou: nenhum solvente residual ou contaminantes e integridade da matriz do polímero após o processo de fundição. A correspondência dos resultados indicou que a interacção enchimento-polímero era adequada e, portanto, os MoO3NPs são potenciais candidatos a serem utilizados como enchimento em matrizes PBAT, especialmente em concentrações em torno de 0,3 %.

Palavras-chave: PBAT, MoO3, filmes nanocompostos, TD-NMR, propriedades estruturais.

1 INTRODUCTION

In the last decade, accumulation of tons of polymeric waste in landfills, rivers and oceans worries society, public authorities, and private institutions. Consequently, scientific research on biodegradable polymers and their composites is conducted to meet demands of plastic products in a more sustainable way. PBAT is an aliphatic/aromatic co-polyester-based biodegradable polymer applied to the agricultural films' industry, compost bags and packaging in general. PBAT has thermoplastic properties, performance and versatility very similar to conventional plastics as polyethylene, with specific advantages such as: high elongation at break and low water vapor permeability, being quite elastic, water and tear resistant, "printable" and suitable to be in contact with food - it's accepted as food package material by FDA [4, 7, 9-11, 13, 16, 22-26].

Studies on hybrid (organic-inorganic) nanocomposites are extremely relevant due to potential for increasing thermal stability, improving barrier properties, increasing dimensional stability, increasing physical and chemical resistance, changing crystallinity, implementing antimicrobial activity, among others. Aiming to achieve polymer matrix improvements, the elements that will compose the nanocomposite, their proportions, and the obtaining method needs to be well-adjusted [2, 5, 8, 27, 28].

Molybdenum oxide (MoO_3) was the nanofiller chosen by its mechanical and chemical properties: very high melting point, a low coefficient of thermal expansion and a high level of thermal conductivity. Thus, MoO_3 nanoparticles (NPs) are an all-rounder filler usable in many different industries. Among all molybdenum compounds, trioxide is

the one produced on a larger scale than all, since it is a very important industrial catalyst. Moreover, MoO_3 NPs exhibits no cytotoxicity and has also been studied as a potential antimicrobial when dispersed in polymeric matrices. When this kind of material is in contact with water molecules, release H^+ ions that form an acidic surface capable of deteriorating cell growth and proliferation. In this way, PBAT/MoO_3 films may represent a potential nanocomposite for active packaging [1, 3, 6, 15, 20, 30].

2 MATERIALS AND METHODS

2.1 MATERIALS

PBAT - ECOFLEX® F Blend C120 (density = 1,25-1,27 g/cm³; melting point = 110-120°C; Mw = 14.2 × 104 g/mol) was received from BASF, BR. Molybdenum oxide (MoO_3 nanopowder) was purchased from Sigma Aldrich, India. Chloroform P.A./ACS (99,8% - stabilized with amylene) were purchased from NEON. All chemicals were used without further purification.

3 FILMS PREPARATION

All films were prepared using solvent evaporation technique, casting. PBAT-$CHCl_3$ solutions were prepared in a 1:25 ratio (w/vol), by adding the preformed polymer to the solvent, at room temperature, ending total dissolution with magnetic stirring for leastwise 30 minutes. After obtaining a homogeneous and clear solution, identical aliquots were collected and poured over glass plates. It took at least 24 hours for the complete removal of $CHCl_3$. Once the pure polymer films were obtained, the incorporation of MoO_3 nanopowder (NPs) into the PBAT solution was tested and performed. PBAT-$CHCl_3$/MoO_3 solutions were prepared with 0.1, 0.3 and 0.5 wt % MoO_3. For nanocomposite casting, the same protocol applied to pure polymer films was followed.

Table 1 - Formulations of PBAT and PBAT/MoO_3 films.

Sample tag	PBAT	MoO_3 (% in mass)
PBAT	pure polymer	–
Mo1	99.9 %	0.1 %
Mo3	99.7 %	0.3 %
Mo5	99.5 %	0.5 %

4 CHARACTERIZATION METHODS

FTIR: All infrared spectra were obtained using a PERKINELMER Frontier FTIR/FIR spectrophotometer (Spectrum version 10.4.2, serial number 98737), with attenuated total reflectance (ATR) accessory, 60 consecutive scans and 4 cm^{-1} resolution within the range of 500–4,000 cm^{-1}. All samples were directly placed on the support after the solvent was completely evaporated.

TGA: Thermogravimetric analysis was carried out using a TGA Q500 DA TA instrument (V20.10 Build 36). All samples were placed in aluminum pans, which were loaded into the equipment. Mass change as a function of temperature was measured by heating the samples from 30 to 700 °C at 10 °C.min^{-1}, under an inert atmosphere (N_2).

XRD: X-ray diffraction studies were performed on a Rigaku Ultima IV X-ray diffractometer (40 kV, 20 mA), using Cu target, at room temperature, in the range of 2θ = 2-50 degree, 0.05º/s.

TD-NMR: Time-domain nuclear magnetic resonance measurements were performed in a Maran Ultra spectrometer with an electromagnetic field of 0.54 T (23.4 MHz for the proton), placed inside 18 mm diameter probes, at room temperature (30 °C). The longitudinal (T_1H) and transverse (T_2H) relaxation times were obtained by inversion recovery (IR) and free induction decay refocused by magic sandwich echo (MSE-FID), respectively. MSE-FID was conducted with up to 1024 data points linearly spaced at intervals of 0.5 microsecond. Experimental points were fitted using WinFit® software, applying one exponential for T_1 and a set of exponential, Gaussian and Abragamian curves for T_2.

5 RESULTS AND DISCUSSION

5.1 FTIR

Pure PBAT film FTIR spectrum showed characteristic stretching bands and peaks matching with the polymer matrix spectra reported in the literature, around 2960; 1720; 1265; 728 cm^{-1} [12, 18, 21]. These data suggests that there were no contaminants, in the polymer or in the solvent, as well as there was no contamination during the casting process.

As can be seen in Figure 1, all nanocomposite films synthesized also showed the characteristic FTIR profile expected for the polymer matrix. The absence of displacements and enlargements in the bands of interest is indicating that there was only physical interaction between system components, keeping its chemical integrity.

Furthermore, this analysis was useful to confirm the total evaporation of chloroform, whose residue, clearly not detected, could be harmful.

Figure 1 - FTIR spectra of pure PBAT and PBAT/MoO_3 films.

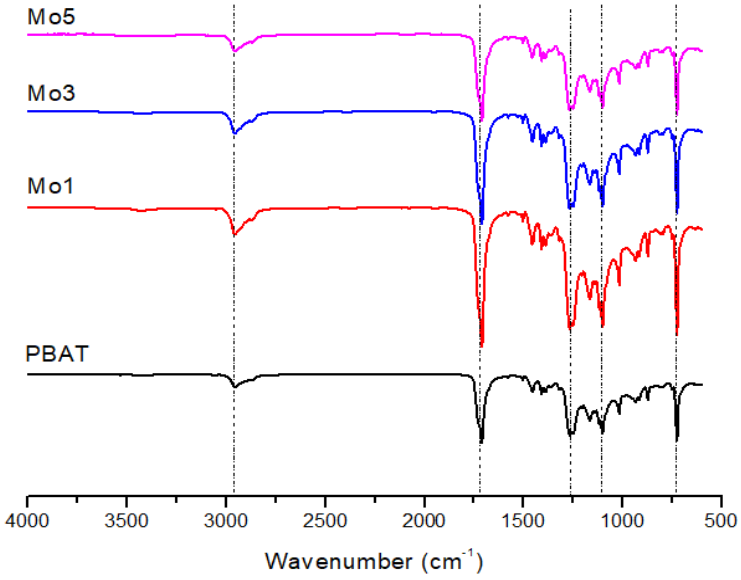

6 TGA

Thermogravimetric analysis (TGA) intended to observe the thermal degradation process suffered by the polymer and its nanocomposites. The results obtained can be seen in Figure 2. Relative mass loss and its derivative (DTGA) were recorded as a function of temperature. PBAT films showed degradation profiles in agreeing with similar results previously reported, performed under similar conditions [14, 19, 27]. Thermal stability increased between 0.1 - 0.3 % MoO_3 NPs. Above that, it was noted a slight heat resistance reduction. These results may be a consequence of good filler dispersion in the systems Mo1 and Mo3, which may have allowed the essentially paramagnetic NPs to absorb the energy, increasing the overall thermal resistivity of the system. With higher NPs' concentrations, on the other hand, the trend was to subtly reduce thermal stability. For Mo5, such reduction could be associated with NPs' agglomeration and poor dispersion of the fillers within polymer matrix. Broadly analyzing the DTGA curves, it can be seen that the presence of molybdenum trioxide caused a more uniform degradation kinetic profile.

Figure 2 - TGA/DTGA curves of pure PBAT and PBAT/MoO_3 films.

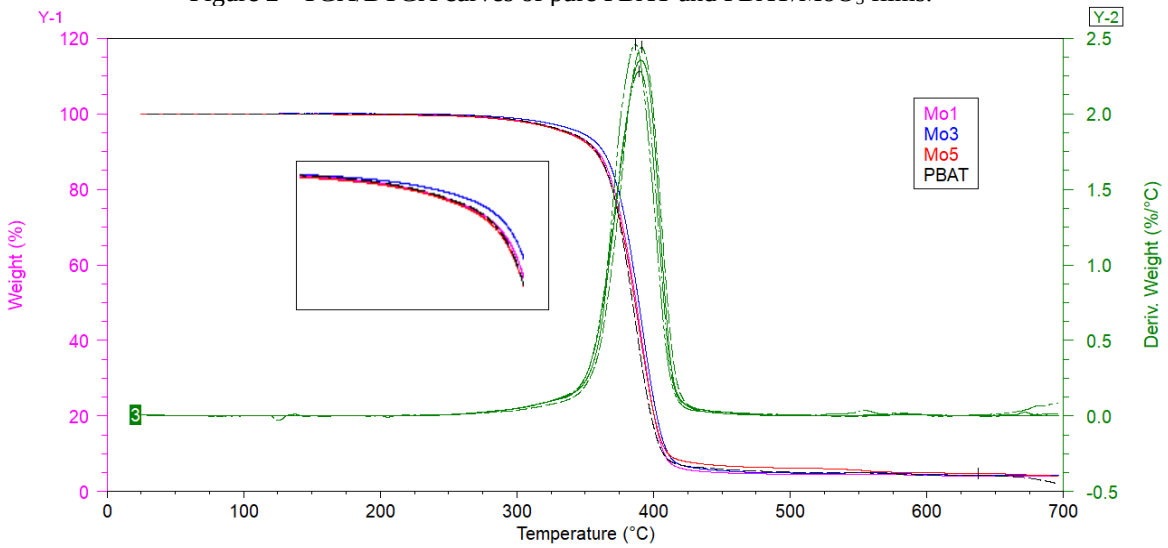

For understanding DTGA data, numerical points of thermal decomposition for pure PBAT and PBAT/MoO_3 films were listed in Table 2. 0.1 % molybdenum NPS was able to increase the thermal resistivity of the matrix only modestly. There was a more expressive increase in T_{onset} for Mo3. T_{peak} values improve for all nanocomposites compared to the pure polymer. Mo3 presented the most satisfactory data regarding the improvement of this thermal property. Mo5 did not demonstrate better thermal performance than Mo3, suggesting that concentrations greater than 0.3 % NPs would not be necessary or even recommended.

Table 2 - Thermal decomposition properties for PBAT and PBAT/MoO_3 films.

Sample	T_{onset} (± 1 °C)	T_{peak} (± 1 °C)
PBAT	364	387
Mo1	366	389
Mo3	369	391
Mo5	364	390

7 XRD

XRD patterns of PBAT nanocomposites are shown with diffraction peaks at 14º, 17°, 20°, 23°, and 25° corresponding to the (010) (110) (100) and (111) planes of PBAT, respectively (Figure 3). PBAT shows its characteristic crystalline planes and its amorphous halo, demonstrating its semi-crystalline characteristic. The X-ray diffraction allows exploring the structure and possible changes in PBAT matrix depending on the prepared nanocomposites, by the position and the shape of the peaks shown in the diffractograms, as well as by the values calculated for the crystallinity degree (Xc) (Table 3). The crystallinity value was calculated by the area equation, where Xc was given by

the ratio between the area of crystalline regions and the total area of the material (amorphous + crystalline), multiplied by 100.

In Figure 3, it is also possible to observe the characteristic peaks of the crystalline planes of molybdenum trioxide. The diffraction pattern of α-MoO_3 confirms the orthorhombic crystalline structure Joint Committee on Powder Diffraction Standards (PASCARIU et al., 2020) with the main diffraction peaks at 23°, 26°, 27°, 30°, indexed by (110), (040), (021) and (130). Systems with higher concentrations of MoO_3NP's have both the matrix and NP crystal planes.

Figure 3 - X-ray diffractograms of PBAT, MoO_3 and PBAT/MoO_3 films.

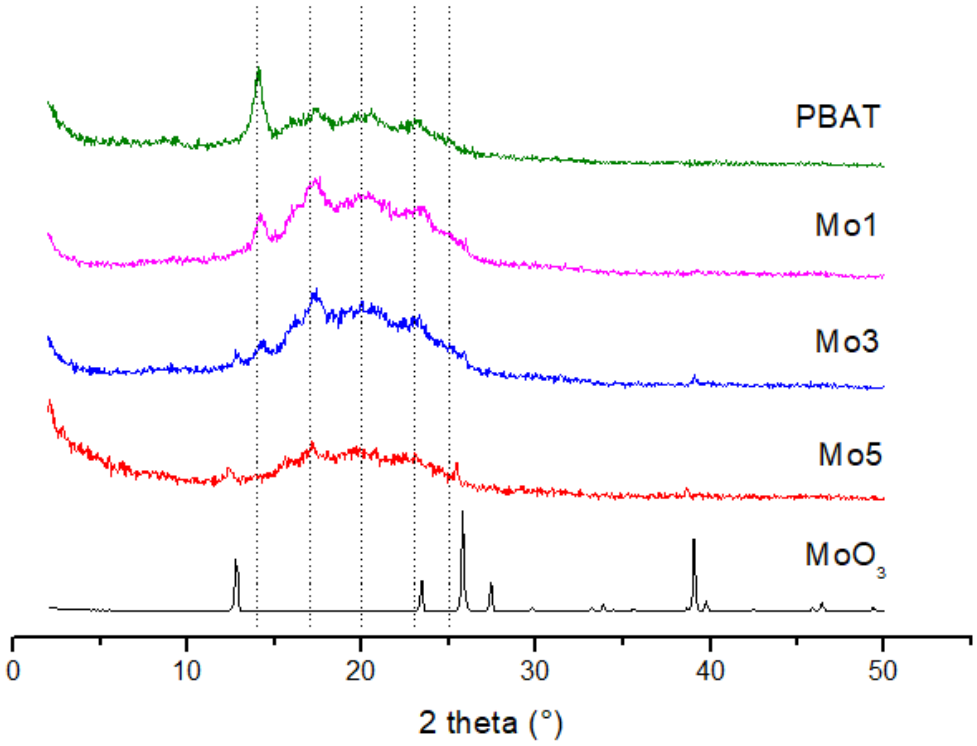

An increase in signals intensity is observed for Mo1 and Mo3 when compared to the other diffractograms, resulting in the highest Xc for both. The observation of peaks around 14º, 17°, 20°, 23°, associated with the crystalline region of PBAT and the absence of peaks associated with molybdenum in Mo1 and Mo3 also suggest a good dispersion of the filler through the polymer matrix.

Table 2 shows that NPs' incorporation made the crystallinity degree more than double for systems Mo1 and Mo3 (129% increase compared to PBAT and Mo5). However, the system with 0.5 % MoO_3NP's did not show this same feature. Possibly, the undue increase in filler concentration may have caused NPs' agglomeration due to the

high affinity between the metal oxide particles, making the system more heterogeneous and expanding its amorphous halo.

Table 3. Crystallinity of pure and nanocomposite films of PBAT/MoO_3 obtained from X-ray data, using the Ruland method

Sample	Crystallinity degree (%) (±1)
PBAT	7
Mo1	16
Mo3	16
Mo5	7

8 TD-NMR

Time-domain nuclear magnetic resonance was used to complement structural study and evaluate the molecular dynamics of the materials. It's an effective unconventional technique with several advantages: non-destructiveness, quick, versatile and provides very sensitive measurements. This relaxometry method can be performed in magnetic fields of different strengths due to determine the relaxation times.

T_1H, the longitudinal relaxation times, which is involved with the return of the magnetization to the thermal equilibrium, was converted into relaxation domain distributions (Figure 4). The spin–lattice relaxation time is sensitive to the intermolecular interactions, which provides information on particles' dispersion, as well as the homogeneity of the system as a whole. As molybdenum is a paramagnetic metal, it interacts with H chains and is expected to decrease relaxation times after its incorporation into polymeric matrices. Indeed, a numerical reduction in relaxation times is only actually observed for Mo3 and Mo5. Possibly, 0.1 % MoO_3NPs was not enough to change the molecular mobility of the sample to the point of shifting T_1H to lower times. Also, analyzing the width of the time domain curves, Mo3 stands out by the greater narrowing of the curve in the main region, signaling superior homogeneity among studied systems. Mo1 showed increased heterogeneity due to its wider base curve and a substantial increase in the second domain time, which can be attributed to larger crystal sizes, corroborating what was denoted by XRD.

Figure 4. Distributions of longitudinal relaxation times domains

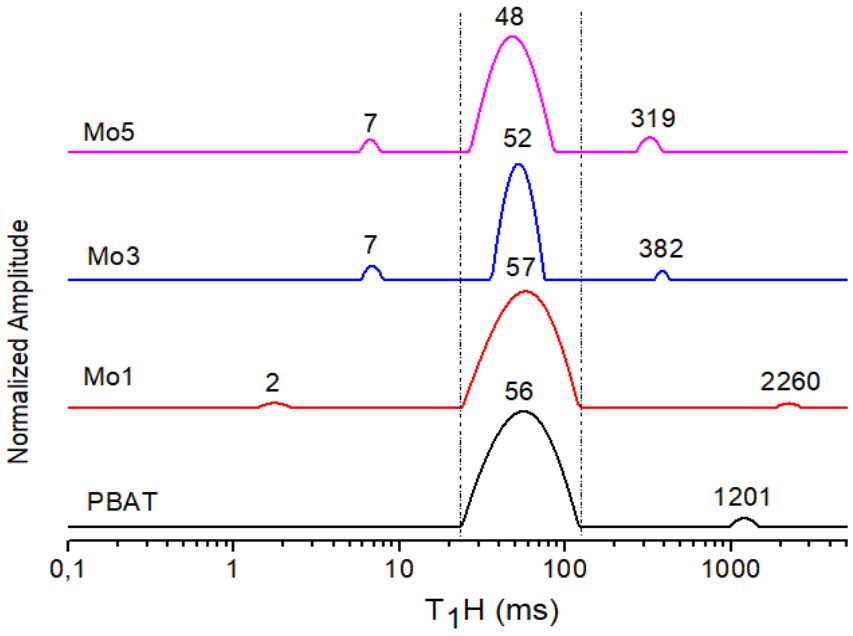

The Mo3 profile may indicate a good NPs dispersion in the amorphous phase or preferentially in one of the polymer phases. In Mo1, the NP dispersion seems to generate multiple interactions, with the NPs being clustered in different ways.

Magic sandwich echo Free Induction Decay (MSE-FID) signal, described in Table 4, was composed of three distinct regions: high rigidity ^{1}H nuclei related to the rigid fraction (F_R), hydrogens at the interface, from semi-rigid mobility (F_{SR}), and, finally, the region of high mobility ^{1}H, that show higher T_2H values (F_M). This technique allows elucidation of much information concerning the crystalline and amorphous regions in each sample. For Mo5, there is a reduction in the mobile fraction, but with higher mobility, a much longer time in the phase of greater mobility. The discussion about crystallinity revolves around the rigid fraction, which is percentage higher in Mo1 and Mo5, but has shorter times especially in Mo3 and, secondarily, Mo5. Thus, one can assume the migration of NPs to one of the matrix phases, preferably.

From the data and correlations of MSE-FID, Mo3 stands out, with better balance in the measured values and, consequently, a better fit of FID (Figure 5), showing that it can represent a better distribution of particles through the polymer.

Figure 5. MSE refocused FIDs for all samples

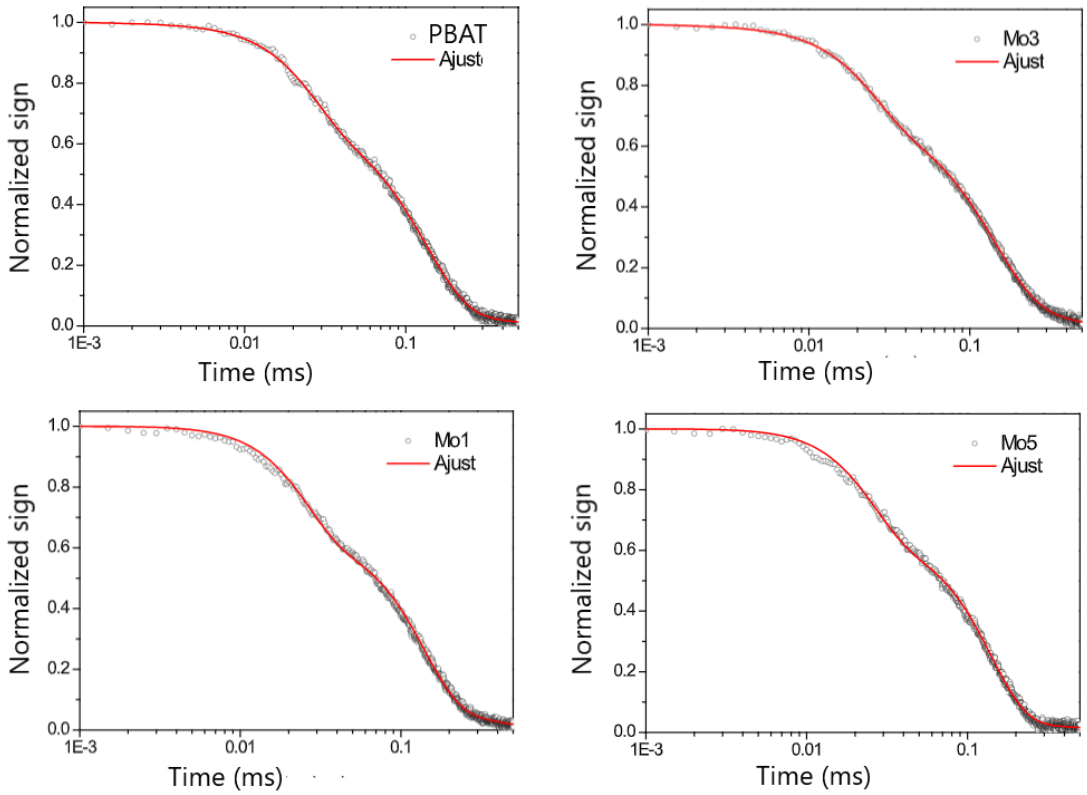

Table 4. Transverse relaxation times of the hydrogen nucleus (T_2) associated with each sample fraction, obtained by MSE-FID

Sample	% F_R	T_{2R} (µs)	% F_{SR}	T_{2SR} (µs)	% F_M	T_{2M} (µs)
PBAT	29	19	59	133	12	157
Mo1	35	21	52	139	13	261
Mo3	26	17	49	142	25	163
Mo5	36	18	59	140	5	498

9 CONCLUSIONS

The FTIR results indicate that the interactions between MoO_3 and PBAT are just physical. Thermogravimetry pointed out improvement in thermal resistance for Mo3. Nonetheless, XRD shows interferences in the crystals plans and in the crystallinity degree from Mo1 and Mo3 in compared to pure PBAT. It could indicate a nucleating action of MoO3 in these concentrations. The time domain analyses show a change in the molecular mobility homogeneity to Mo3 and Mo5.

The homogeneity change was most pronounced in Mo3, indicating a possible agglomeration or bad distribution of nanofiller in Mo5. MoO_3NPs changed the dynamic of systems molecular mobility and the crystallinity process, promoting an increase in some crystals plans, specially in Mo3. The results pointed to Mo3 as the most promising system in this context.

STATEMENTS AND DECLARATIONS

We acknowledge IMA, UFRJ. Additionally, we would like to thank the funding agencies that supported this research: Conselho Nacional de Desenvolvimento Científico e Tecnológico – CNPq, Coordenação de Aperfeiçoamento de Pessoal de Nível Superior – Capes and Fundação de Amparo à Pesquisa do Estado do Rio de Janeiro – FAPERJ.

REFERENCES

1. BALENDHRAN, S. et al. Two-Dimensional Molybdenum Trioxide and Dichalcogenides. Advanced Functional Materials. 2013; https://doi.org/10.1002/adfm.201300125

2. BODAGHI, H. et al. Evaluation of the photocatalytic antimicrobial effects of a TiO2 nanocomposite food packaging film by in vitro and in vivo tests. LWT - Food Science and Technology. 2013; http://dx.doi.org/10.1016/j.lwt.2012.07.027

3. BOŽINOVI, K. et al. In-vitro toxicity of molybdenum trioxide nanoparticles on human keratinocytes. Elsevier. 2020; https://doi.org/10.1016/j.tox.2020.152564

4. BRITO, G. F. et al. Biopolímeros, Polímeros Biodegradáveis e Polímeros Verdes. Revista Eletrônica de Materiais e Processos. , v. 6, n. 2, p. 127–139, 2011. ISSN 1809-8797

5. EMAMIFAR, A. et al. Evaluation of nanocomposite packaging containing Ag and ZnO on shelf life of fresh orange juice. Innovative Food Science & Emerging Technologies. 2010; http://dx.doi.org/10.1016/j.ifset.2010.06.003

6. FAZELIPOUR, S. et al. Effect of molybdenum trioxide nanoparticles on histological changes of uterus and biochemical parameters of blood serum in rat. 2020; https://doi.org/10.1007/s00580-020-03137-5

7. FRANCHETTI, S. M. M.; MARCONATO, J. C. Polímeros biodegradáveis - Uma solução parcial para diminuir a quantidade dos resíduos plásticos. Quimica Nova. 2006; https://doi.org/10.1590/S0100-40422006000400031

8. FUKUSHIMA, K.; RASYIDA, A.; YANG, M. C. Characterization, degradation and biocompatibility of PBAT based nanocomposites. Applied Clay Science. 2013; https://doi.org/10.1590/0370-44672018720077

9. HAIDER, T. P. et al. Plastics of the Future? The Impact of Biodegradable Polymers on the Environment and on Society. Angewandte Chemie - International Edition. 2019; https://doi.org/10.1002/anie.201805766

10. IWATA, T. Biodegradable and bio-based polymers: Future prospects of eco-friendly plastics. Angewandte Chemie - International Edition. 2015; https://doi.org/10.1002/anie.201410770

11. JARAMILLO, A. F. et al. Comparative Study of the Antimicrobial Effect of Nanocomposites and Composite Based on Poly(butylene adipate-co-terephthalate) Using Cu and Cu/Cu 2 O Nanoparticles and CuSO 4. Nanoscale Research Letters. 2019; https://doi.org/10.1186/s11671-019-2987-x

12. JIANG, G. et al. Structure and improved properties of PPC/PBAT blends via controlling phase morphology based on melt viscosity. Journal of Applied Polymer Science. 2020; https://doi.org/10.1002/app.48924

13. LAMBERT, S.; WAGNER, M. Environmental performance of bio-based and biodegradable plastics: The road ahead. Chemical Society Reviews. 2017; https://doi.org/10.1039/c7cs00149e

14. LI, G. et al. An Investigation of the thermal degradation of the intumescent coating containing MoO_3 and Fe_2O_3. Surface and Coatings Technology. 2008; http://dx.doi.org/10.1016%2Fj.surfcoat.2007.11.016

15. MARIMUTHU, M. et al. Methylene Blue-Fortified Molybdenum Trioxide Nanoparticles: Harnessing Radical Scavenging Property. ACS Publications. 2018; https://doi.org/10.1021/acsami.8b15841

16. MOUSTAFA, H. et al. PLA/PBAT bionanocomposites with antimicrobial natural rosin for green packaging. ACS Applied Materials and Interfaces. 2017; https://doi.org/10.1021/acsami.7b05557

17. PASCARIU, P. et al. New Electrospun ZnO:MoO3 Nanostructures: Preparation, Characterization and Photocatalytic Performance. Nanomaterials. 2020; https://doi.org/10.3390/nano10081476

18. REN, Y. et al. Biodegradation Behavior of Poly (Lactic Acid) (PLA), Poly (Butylene Adipate-Co-Terephthalate) (PBAT), and Their Blends Under Digested Sludge Conditions. Journal of Polymers and the Environment. 2019; https://link.springer.com/article/10.1007/s10924-019-01563-3

19. RIZZARELLI, P. et al. Determination of polyethylene in biodegradable polymer blends and in compostable carrier bags by Py-GC/MS and TGA. Journal of Analytical and Applied Pyrolysis. 2016; https://doi.org/10.1016/j.jaap.2015.12.014

20. SEBENIK, R. F. et al. Molybdenum and Molybdenum Compounds. In: Ullmann's Encyclopedia of Industrial Chemistry. 2000; https://doi.org/10.1002/14356007.a16_655.pub2

21. SIYAMAK, S. et al. Effect of Fiber Esterification on Fundamental Properties of Oil Palm Empty Fruit Bunch Fiber/Poly(butylene adipate-co-terephthalate) Biocomposites. International Journal of Molecular Sciences. 2012; https://doi.org/10.3390/ijms13021327

22. TOUCHALEAUME, F. et al. Performance and environmental impact of biodegradable polymers as agricultural mulching films. Chemosphere. 2016; https://doi.org/10.1016/j.chemosphere.2015.09.006

23. VASILE, C. Polymeric Nanocomposites and Nanocoatings for Food Packaging: A Review. Materials. 2018; https://dx.doi.org/10.3390%2Fma11101834

24. VENKATESAN, R.; RAJESWARI, N. TiO_2 nanoparticles/poly(butylene adipate-co-terephthalate) bionanocomposite films for packaging applications. Polymers for Advanced Technologies. 2017; https://doi.org/10.1002/pat.4042

25. WANG, B. et al. Interlayer Engineering of Molybdenum Trioxide toward High-Capacity and Stable Sodium Ion Half/Full Batteries. Advanced Functional Materials. 2020; https://doi.org/10.1002/adfm.202001708

26. WANG, H. et al. Soil burial biodegradation of antimicrobial biodegradable PBAT films. Polymer Degradation and Stability. 2015; https://doi.org/10.1016/j.polymdegradstab.2015.03.007

27. XIANG, S. et al. Evaluation of PLA content in PLA/PBAT blends using TGA.

Polymer Testing. 2020; https://doi.org/10.1016/j.polymertesting.2019.106211

28. YOUSSEF, A. M. Polymer Nanocomposites as a New Trend for Packaging Applications. 2013; https://doi.org/10.1080/03602559.2012.762673

29. ZEHETMEYER, G. et al. Influence of melt processing on biodegradable nisin-PBAT films intended for active food packaging applications. Journal of Applied Polymer Science. 2016; https://doi.org/10.1002/APP.43212

30. ZOLLFRANK, C. et al. Antimicrobial activity of transition metal acid MoO_3 prevents microbial growth on material surfaces. Materials Science and Engineering. 2012; https://doi.org/10.1016/j.msec.2011.09.010